ACS APPLIED NANO MATERIALS
Cite This: ACS Appl. Nano Mater. 2019, 2, 2881−2889
Article
www.acsanm.org

High Defect Nanoscale ZnO Films with Polar Facets for Enhanced Photocatalytic Performance

Premrudee Promdet,[†] Raul Quesada-Cabrera,[†] Sanjayan Sathasivam,[†] Jianwei Li,[†] Arreerat Jiamprasertboon,[†,‡] Jian Guo,[†] Alaric Taylor,[§] Claire J. Carmalt,[†] and Ivan P. Parkin*[,†]

[†]Materials Chemistry Centre, Department of Chemistry, University College London, 20 Gordon Street, London WC1H 0AJ, U.K.
[‡]School of Chemistry, Institute of Science, Suranaree University of Technology, 111 University Avenue, Muang, Nakhon Ratchasima 30000, Thailand
[§]Department of Electronic & Electrical Engineering, University College London, Torrington Place, London WC1E 7JE, U.K.

Supporting Information

ABSTRACT: The fabrication of highly efficient photocatalytic thin films has important consequences for self-cleaning, organic pollutant decomposition, and antimicrobial coatings for a variety of applications. Here, we developed a simple synthesis method to produce efficient, high-surface-area zinc oxide (ZnO) photocatalytic films using aerosol-assisted chemical vapor deposition. This approach used mixtures of methanol and acetic acid to promote preferential growth and exposure of polar facets, which favor photocatalytic activity. Interestingly, the initial enhanced efficiency of the films was correlated to structural defects, likely oxygen vacancies, as supported by photoluminescence spectroscopy results. Discussion over the influence of such defects on photocatalytic performance is described, and the need for strategies to develop high-surface-area materials containing stable defects is highlighted.

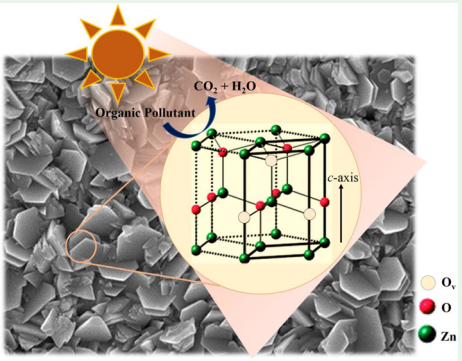

KEYWORDS: *ZnO, photocatalyst, AACVD, polar facets, oxygen vacancies*

1. INTRODUCTION

Oxide semiconductors have attracted interest as an effective material for photocatalyst applications because of their high photocatalytic activity and mechanical and chemical durability.[1] ZnO, a wide band gap material with a band gap of 3.37 eV and a large excitonic binding energy of 60 meV at room temperature, has been considered a promising material in photocatalysis,[2−6] which can be used for degradation of organic pollutants[7−9] and photolysis of water to generate hydrogen.[10−12] Moreover, ZnO possesses generally hydrophilic surfaces (water contact angle $\theta < 90°$)[13,14] and environmentally friendly features.

Synthesis routes to highly textured or nanostructured metal-oxide films have attracted attention since these materials often show enhanced functional properties compared to flat conventional thin films. For example, one-dimensional ZnO nanostructures, such as nanotubes and nanowires, are attractive for applications in piezoelectric generators,[15] UV photodetectors,[16] and solar cells.[17] Two-dimensional hexagonal ZnO nanoplates have also shown enhanced activities for gas sensing[18] and photocatalysis applications.[4,5,19] The photocatalytic properties of semiconductor materials are strongly determined by their morphology. For example, it has been reported that a morphology that exposes polar surfaces can lead to an enhancement in the photodegradation of organic pollutants.[19−21] There are three main morphologies related to surfaces in wurtzite ZnO, namely, the nonpolar $\{10\bar{1}0\}$, semipolar $\{10\bar{1}1\}$, and polar {0001} facets. The latter intrinsically holds high surface energy and strategies to maximize the {0001} surface area are often followed in the synthesis of optimized ZnO materials, such as inducing preferential growth along the ⟨001⟩ or *c*-axis.[22−27] In a photocatalytic reaction, OH^- ions preferentially adsorb onto the (0001)-Zn surface because of its surface positive charge, favoring formation of ·OH radicals and thus promoting activity.[28]

Among the large number of synthesis methods to produce ZnO materials, the synthesis of thin films is widely convenient for practical applications. An extensive variety of deposition techniques can be used to produce ZnO films, including pulse laser deposition,[29] molecular beam epitaxy,[30] thermal evaporation,[31] chemical vapor deposition,[32] and RF magnetron sputtering,[33] among others. Each one of these techniques has advantages and disadvantages, which include high costs, long reaction times, the use of toxic templates, poor control over physical properties, and so on. Aerosol-assisted chemical vapor deposition (AACVD) is a rather simple, scalable, and cost-efficient technique that allows good control over physical properties (crystallinity, film thickness, morphology).[34−37] In AACVD, precursors with low vapor pressure are dissolved in

Received: February 20, 2019
Accepted: May 3, 2019
Published: May 3, 2019

DOI: 10.1021/acsanm.9b00326
ACS Appl. Nano Mater. 2019, 2, 2881−2889

an appropriate solvent, and the resulting solution is aerosolized and transported into the CVD chamber using a carrier gas. The solvent is not only a vehicle to transport the precursors to the substrate but can also be a key reagent in itself. Thus, the solvent of choice can play a crucial role in influencing the physical properties of the film.[36,38,39]

In the current work, AACVD was used to synthesize highly textured ZnO films from mixtures of zinc acetate dihydrate, methanol, and acetic acid. Adding acetic acid to the precursor solution had an important influence in controlling the morphology of the films by favoring particle growth along the *c*-axis. The corresponding photocatalytic activities of the as-deposited films could be explained by the change in the specific surface areas; however, their photocatalytic behavior after annealing was somehow unexpected. Changes in photocatalytic properties were further investigated using photoluminescence spectroscopy (PL). PL studies can provide valuable information about surface defects, electronic structure, and charge carrier processes in semiconductor materials.[40] The presence of surface defects, such as oxygen vacancies, can have a huge impact on photocatalytic efficiency since they can promote separation of photogenerated excitons and thus contribute toward charge carrier lifetimes.[41,42] Furthermore, the injection of photogenerated electrons into oxygen molecules favorably adsorbed in the vicinity of oxygen vacancy sites can promote formation of ·OH radicals, which have a major role on the photocatalytic process. The implementation of similar synthesis routes rendering defected materials with high surface area is key toward industrial applications of thin films.

2. EXPERIMENTAL SECTION

2.1. Thin Film Synthesis. All chemicals were used as received from Sigma-Aldrich. ZnO thin films were deposited from zinc acetate dihydrate (98%) and mixtures of acetic acid (99%) and methanol (anhydrous, 99.8%) using aerosol-assisted chemical vapor deposition (AACVD). In this system, a precursor mist was formed using an ultrasonic humidifier (Johnson Matthey) and introduced in the reaction chamber under a controlled flow of nitrogen gas (1.0 L min^{-1}). The deposition of ZnO films was performed at an optimized temperature of 400 °C on silica-barrier floating glass substrates (NSG Pilkington Ltd.). Each deposition was completed within 50 min. All films were well adherent to the substrate, passing the Scotch tape test.[43]

2.2. Analytical Methods. Film morphology and thickness were studied using top- and side-view scanning electron microscopy (SEM) in a JEOL6301 instrument (10 kV). X-ray diffraction (XRD) analysis was performed using a Bruker-Axs D8 (GADDS) diffractometer. The instrument operated with a monochromated Cu X-ray source with Cu $K\alpha_1$ (λ = 1.54056 Å) and Cu $K\alpha_2$ radiation (λ = 1.54439 Å) emitted with an intensity ratio of 2:1 and a 2D area X-ray detector with a resolution of 0.01°. Films were analyzed with a glancing incident angle (θ) of 1°. The diffraction patterns obtained were refined using database standards. UV/vis spectroscopy was performed using a double monochromated PerkinElmer Lambda 950 UV/vis/NIR spectrophotometer in the 300−800 nm range. X-ray photoelectron spectroscopy (XPS) was performed on a Thermo K alpha spectrometer with monochromated Al Kα radiation, a dual beam charge compensation system at a pass energy of 50 eV. Survey scans were performed between 0 and 1200 eV. High-resolution XPS spectra were used for the principal peaks of Zn (2p) and fitted using CasaXPS software with the calibration of C 1s at 284.5 eV. Room temperature photoluminescence (Renishaw 1000) spectroscopy was employed to study the optical properties of the ZnO films using a He−Cd laser with a wavelength of 325 nm. The surface roughness of films was characterized by atomic force microscopy (AFM) on a Keysight 5600LS scanning probe microscope taken at a scale of 10 × 10 μm^2.

2.3. Photocatalytic Test. The intrinsic photocatalytic properties of the films were investigated during photodegradation of octadecanoic (stearic) acid (95%), which is used here as a model organic pollutant.[44] Stearic acid is very stable under UVA irradiation in the absence of a photocatalyst and the photocatalytic degradation (solid−gas reaction) conveniently follows zero-order reaction kinetics above a critical concentration of the acid. In these experiments, the films were dip-coated with a thin layer of stearic acid from a 0.05 M solution in chloroform and then monitored under UVA irradiation over a period of 24 h using a PerkinElmer RX-I Fourier transform infrared (FTIR) spectrometer. Plots of integrated areas of characteristic C−H infrared bands at 2958, 2923, and 2853 cm^{-1} were produced, and the photodegradation rates were estimated from linear regression of the initial 30−50% of the curves. A conversion factor from the literature (1 $cm^{-1} \equiv 9.7 \times 10^{15}$ molecules of stearic acid)[45] allowed for the estimation of the number of molecules of stearic acid degraded upon irradiation time. The light source used was a UVA (λ = 365 nm) Vilber-Lourmat BLB lamp (2 × 8 W, I = 1.0 mW cm^{-2}). The irradiance of the lamp was measured using a UVX radiometer (UVP).

3. RESULTS AND DISCUSSION

The deposition of ZnO thin films was performed using aerosol-assisted chemical vapor deposition AACVD as detailed in the Experimental Section. First, the vaporized precursor solution (zinc acetate dihydrate, acetic acid, and methanol) is transported to tube furnace using nitrogen as carrier gas.

On heated substrate, the precursors react followed by the deposition of ZnO. Meanwhile, the waste products are carried away to the exhaust as shown in Scheme 1.

Scheme 1. Illustration of Principle of AACVD Operation Used for ZnO Deposition

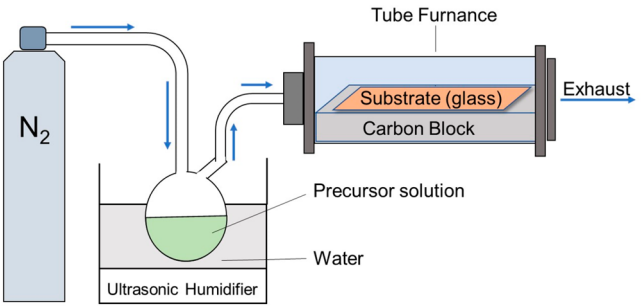

The precursor solutions contained 0.6 g of zinc acetate dihydrate dissolved in 60 mL of methanol and additional volumes of acetic acid (0, 1, 2, or 8 mL, corresponding to 0, 1.64, 3.23, and 11.76 vol %, respectively, henceforth Z-0, Z-1.64, Z-3.23, and Z-11.76). The as-prepared ZnO films showed good adherence and excellent mechanical stability, and the additional volumes of acetic acid had a large impact on particle growth and the microstructure of the films (Figure 1).

The untreated ZnO film showed regular spherical particles with average size of ca. 80 nm. The addition of 1.64 vol % of acetic acid into the precursor solution favored particle growth to an average size of ca. 300 nm. Further additional volumes of acid (3.23 vol %) resulted in films exhibiting hexagonal plates of different sizes. Upon addition of 11.76 vol % of acetic acid, the films showed large distorted plates. Surface topography of the ZnO films was investigated by AFM, taken at a scale of 10 × 10 μm^2 as shown in Figure 2. The AFM topography reveals that with increasing acetic acid concentration the film surface area and surface roughness also increase. The surface area of

DOI: 10.1021/acsanm.9b00326
ACS Appl. Nano Mater. 2019, 2, 2881−2889

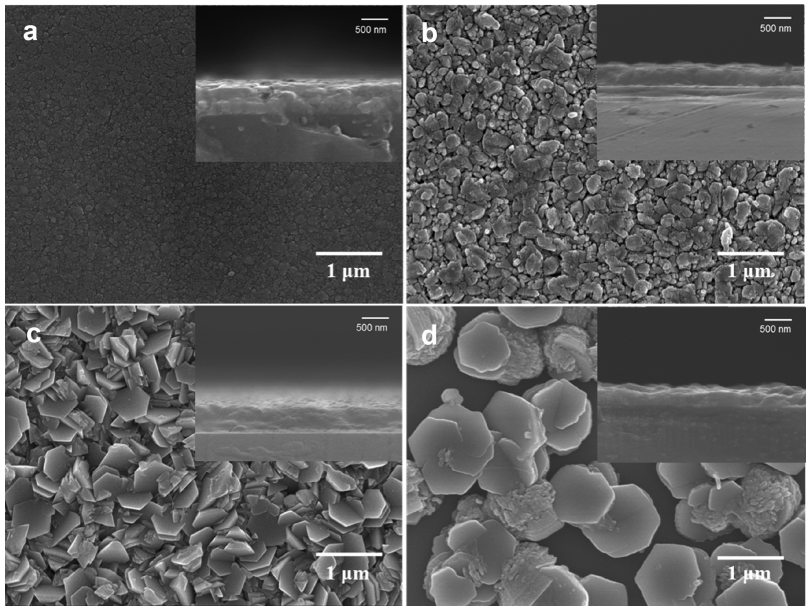

Figure 1. Scanning electron microscopy (SEM) images showing the impact of different mixtures of methanol and acetic acid on the microstructure of the ZnO films. The additional volumes of acetic acid were (a) 0 mL (0 vol %), (b) 1 mL (1.64 vol %), (c) 2 mL (3.23 vol %), and (d) 8 mL (11.76 vol %). Inset figures show corresponding side-on views.

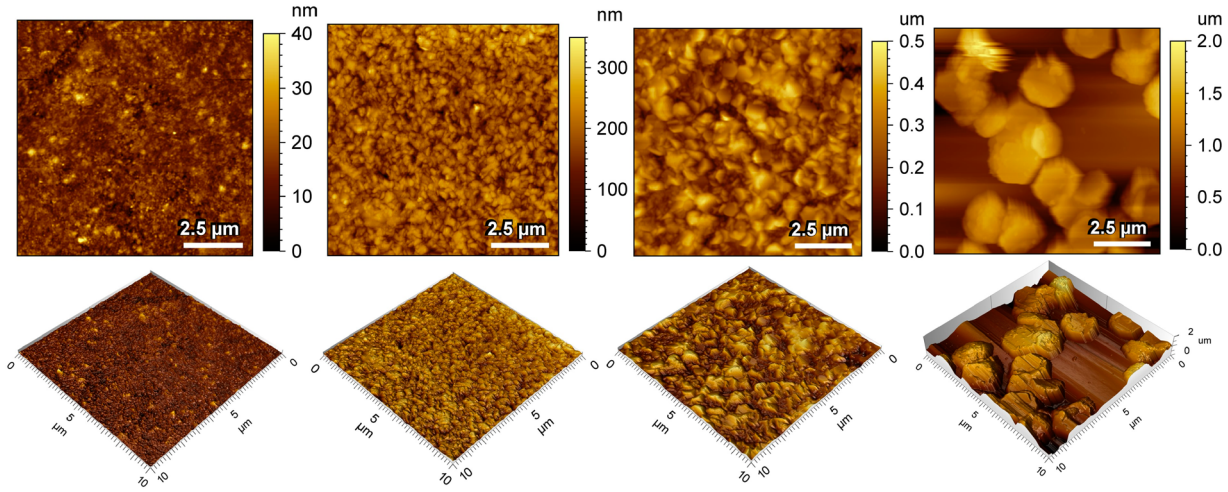

Figure 2. AFM images of ZnO thin films coated on glass. (a) 2D (top) and (b) 3D (bottom) images of the surface of prepared ZnO films (a) Z-0, (b) Z-1.64, (c) Z-3.23, and (d) Z-11.76, respectively, at a scale of 10 × 10 μm^2.

Table 1. Structural, Optical, and Functional Parameters of ZnO Films from Different Mixtures of Methanol and Acetic Acid in the Precursor Mixture

	acetic acid						ξ (molecules photon^{-1})	
sample	(mL)	(vol %)	film thickness (nm)	E_{bg} (eV)	surface area (μm^2)	rms roughness (nm)	as-dep	anneal
Z-0	0	0	700	3.3	102	60	1.1	1.2
Z-1.64	1	1.64	470	3.3	120	67	3.1	0.8
Z-3.23	2	3.23	480	3.3	129	135	6.9	1.0
Z-11.76	8	11.76	290	3.3	160	354	4.2	1.2

untreated ZnO film was 102 μm^2, and treated ZnO films (1.64, 3.23, and 11.76 vol %) possessed 120, 129, and 160 μm^2, respectively. The surface roughness (rms roughness) of the 11.76 vol % increased more than 5 times compared with the untreated films (Table 1).

These film morphologies correlated to previous observations[46,47] and are determined by the grain growth process that occurs after the nucleation step during CVD. In the absence of acetic acid, the growth rate along the *c*-axis is similar to that of the radial axis (growing equivalent planes), thus resulting in small round particles.[48,49] However, upon addition of acetic acid, the selective adsorption of acetate anions on the {0001} facets inhibited crystal growth along the *c*-axis and promoted growth along the *a*-axis, with formation of hexagonal plates.[47,50] Furthermore, side-on SEM analysis (Figure 1,

DOI: 10.1021/acsanm.9b00326
ACS Appl. Nano Mater. 2019, 2, 2881−2889

Scheme 2. Alcoholysis Ester Elimination Reaction between Zinc Acetate and Methanol To Form $Zn(OH)_2$ and Methyl Acetate[51]

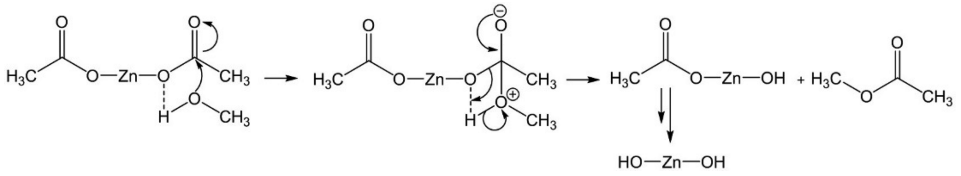

inset) showed film thicknesses decreasing from ca. 700 nm (0 vol %) to 290 nm (11.76 vol %) (Table 1).

This effect was attributed to a decrease in zinc hydroxide molecules ($Zn(OH)_2$) upon increasing volumes of acetic acid in the precursor solutions. This phenomenon might result from the excess CH_3COO^- anions and H^+ (eq 3) upon the addition of acetic acid to the precursor solutions, reducing free methanol in the precursors by promoting eq 4 to proceed to the right side and decrease the ester elimination reaction, which might reduce $Zn(OH)_2$. The ester elimination reaction could take place between zinc acetate and methanol to form $Zn(OH)_2$ and methyl acetate.[51] Dehydration of $Zn(OH)_2$ is important in the formation of crystalline ZnO and would generate nucleation points.[51]

$$Zn(CH_3COO)_2 \xrightarrow{2CH_3OH} Zn(OH)_2 + 2CH_3COOCH_3 \quad (1)$$

$$Zn(OH)_2 \xrightarrow{\text{heating}} ZnO + H_2O\uparrow \quad (2)$$

$$CH_3COOH \xleftrightarrow{\text{equilibrium}} H^+ + CH_3COO^- \quad (3)$$

$$CH_3OH + H^+ \xleftrightarrow{\text{equilibrium}} CH_3OH_2^+ \quad (4)$$

Less $Zn(OH)_2$ can reduce the ZnO nucleation rate and the number of nucleation sites. Thus, the crystals in acid-treated ZnO samples could obtain more lateral space to grow and have larger grain sizes.

Examination of the Zn 2p core level XPS spectra of all ZnO films showed the Zn $2p_{3/2}$ peak at 1021.7 eV corresponding to Zn in the 2+ oxidation state.[52] X-ray diffraction analysis confirmed the presence of hexagonal wurtzite ZnO phase (*P*63*mc* space group, a = 3.2490 Å, b = 3.2490 Å, and c = 5.2050 Å; ICCD Card No. 5-0664) and the preferential growth in the films with relatively high concentration of acetic acid in the precursor solution (Figure 3a).

The preferential growth of a particular plane can be represented by the texture coefficient (TC), expressed as[53,54]

$$TC = \frac{I(hkl)/I_0(hkl)}{n - 1\sum_{i=1}^{i=n} I(hkl)/I_0(hkl)}$$

where the condition for preferential growth is observed in diffraction peaks with TC > 1. In this equation, $I(hkl)$ and $I_0(hkl)$ are peak intensities of a sample and reference (JCPDS data card 01-1136), respectively, and n is the number of diffraction peaks considered. The TC values calculated for different orientations in the ZnO films are shown in Figure 3b.

The untreated sample exhibited broad, weak diffraction peaks, as may be expected from diffraction of nanoparticles (80 nm), although it can also be due to relatively poor crystallinity. In the absence or at relatively low concentrations (1.64 vol %) of acetic acid in the precursor mixtures, the resulting films showed TC values above 1 for several peaks, indicating

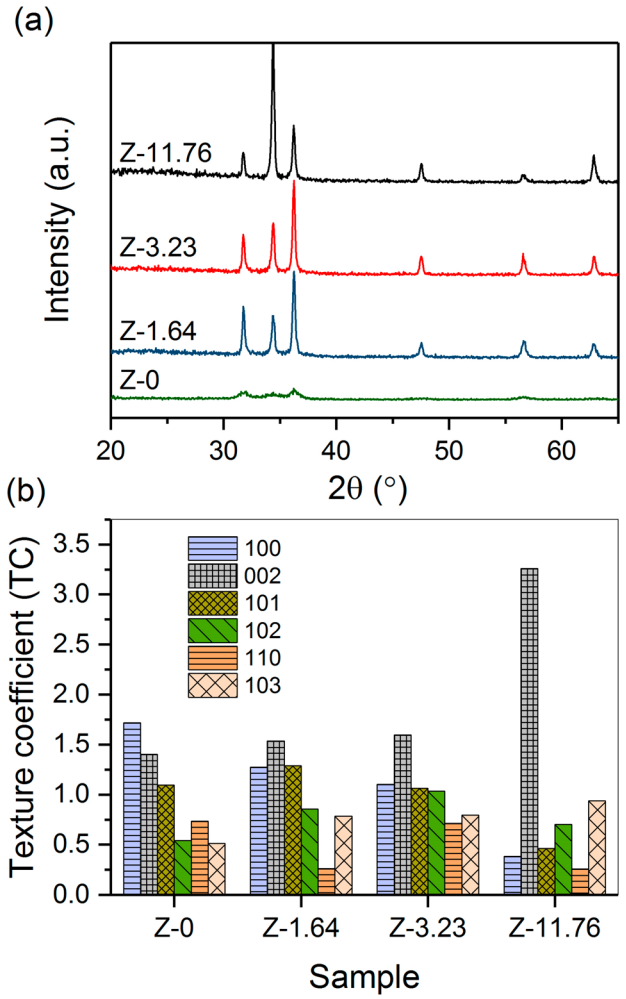

Figure 3. (a) X-ray diffraction analysis and (b) corresponding texture coefficients of ZnO films prepared with different mixtures of methanol and acetic acid. The additional volumes of acetic acid into the precursor mixtures were (a) 0 mL (0 vol %), Z-0; (b) 1 mL (1.64 vol %), Z-1.64; (c) 2 mL (3.23 vol %), Z-3.23; and (d) 8 mL (11.76 vol %), Z-11.76.

relatively random orientation of the particles, as observed in the SEM images (Figure 1). Higher concentrations of acetic acid, however, encouraged preferential growth in the (002) plane, with the highest TC value of 3.26 for the 11.76 vol % sample.

With respect to optical properties, all films showed high transparency to the visible range (Figure 4). Diffuse transmission spectra changed from <10% (0 vol %) to >70% (11.76 vol %), which resulted in increasing haze factors and a strong light trapping ability upon addition of acetic acid in the precursor mixture (Table 1) as well as enhancing light absorption as shown is Figure S1. Noticeably, Z-11.76 provide

DOI: 10.1021/acsanm.9b00326
ACS Appl. Nano Mater. 2019, 2, 2881−2889

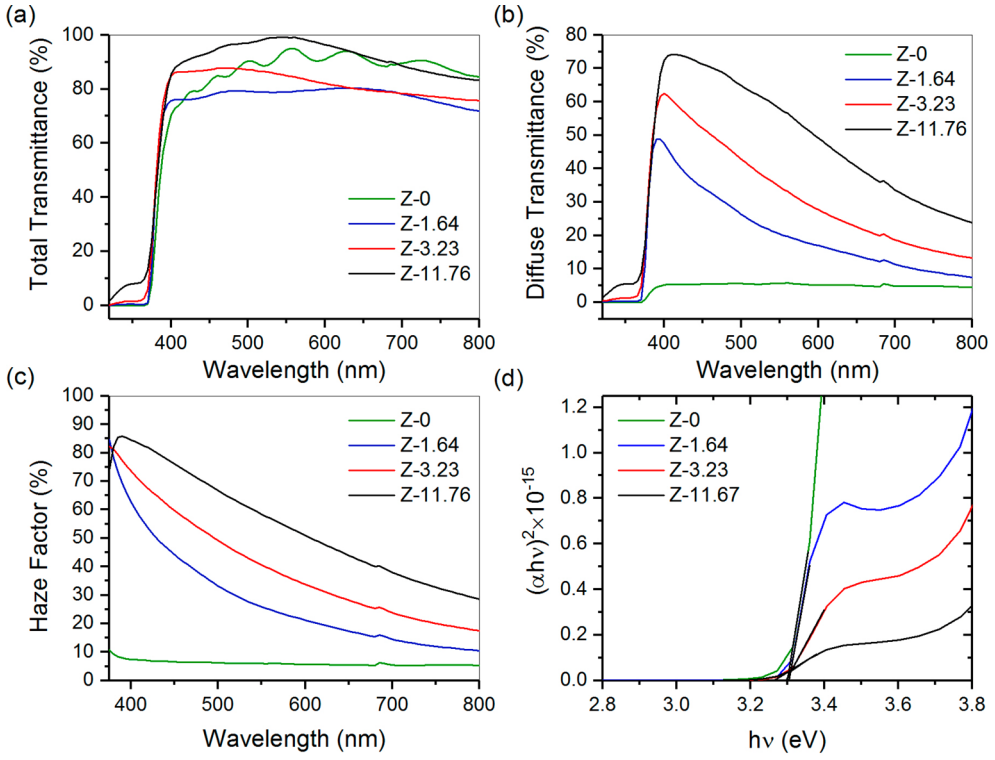

Figure 4. (a) Total and (b) diffuse transmittance of the ZnO films as deposited from different mixtures of methanol and acetic acid. (c) Haze factor and (d) Tauc plots allowing an estimation of band gap energies of ZnO films prepared with different mixtures of methanol and acetic acid. The additional volumes of acetic acid into the precursor mixtures were (a) 0 mL (0 vol %), Z-0; (b) 1 mL (1.64 vol %), Z-1.64; (c) 2 mL (3.23 vol %), Z-3.23; and (d) 8 mL (11.76 vol %), Z-11.76.

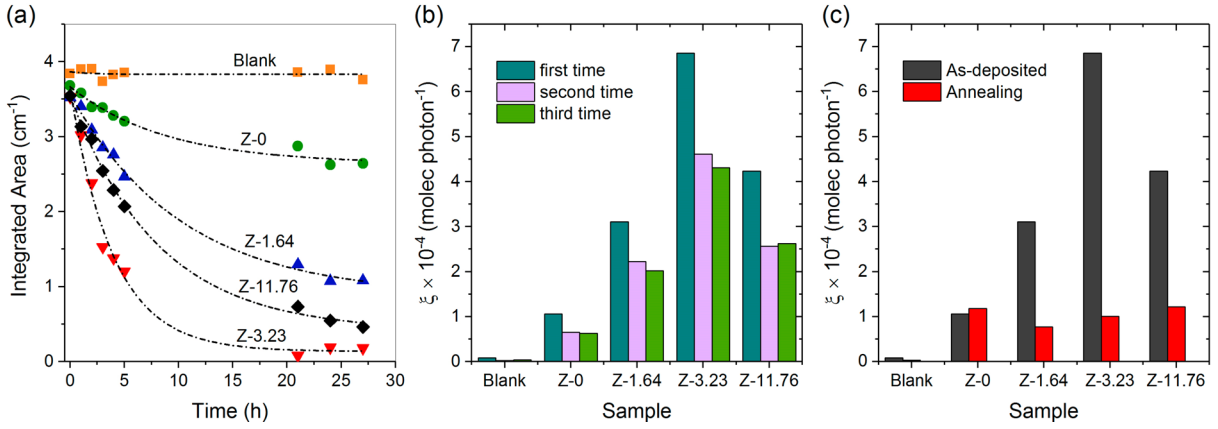

Figure 5. (a) Integrated areas of the IR spectra of stearic acid upon irradiation time (UVA, λ = 365 nm, I = 1.0 mW cm^{-2}). (b) Corresponding formal quantum efficiencies (ξ), given as molecules degraded per incident photon (units, molecules photon^{-1}), upon cycle experiments. (c) ξ values before and after annealing to 500 C for 6 h in air. A blank reference corresponds to the glass substrate without the photocatalytic coating.

the highest transparency; otherwise, the absorption spectrum of the films is higher than Z-0 resulting from surface roughness. High surface roughness results in the reduction of reflectance and enhancing of absorption.

The onset of absorption edges was observed at approximately λ = 370 nm (Figure 4), resulting from the characteristic band gap absorption of ZnO. Band gap energy (E_{bg}) values ranged from 3.29 to 3.33 eV (Table 1), as estimated via the Tauc model for a direct band gap transition.[55]

The photocatalytic properties of the ZnO films were evaluated from the degradation of stearic acid under UVA irradiation (λ= 365 nm, I = 1.0 mW cm^{-1}). The corresponding degradation curves are plotted against irradiation time in Figure 5a. The trend of degradation curves was as expected with high-surface-area samples (3.23 and 11.76 vol %) being the most effective photocatalysts. In the case of Z-3.23, full mineralization was reached within 24 h of irradiation. The fitting of the initial degradation steps (zero-order kinetics) allowed for the estimation of formal quantum efficiencies (ξ, units molecules photon^{-1}), given as number of acid molecules degraded per incident photon (Figure 5b).[56]

The influence of any particular crystallographic plane exposed to the media could not be established unambiguously in these experiments; however, Vallejos et al.[52] attributed the efficient photocatalytic performance of the hexagonal plates as

DOI: 10.1021/acsanm.9b00326
ACS Appl. Nano Mater. 2019, 2, 2881−2889

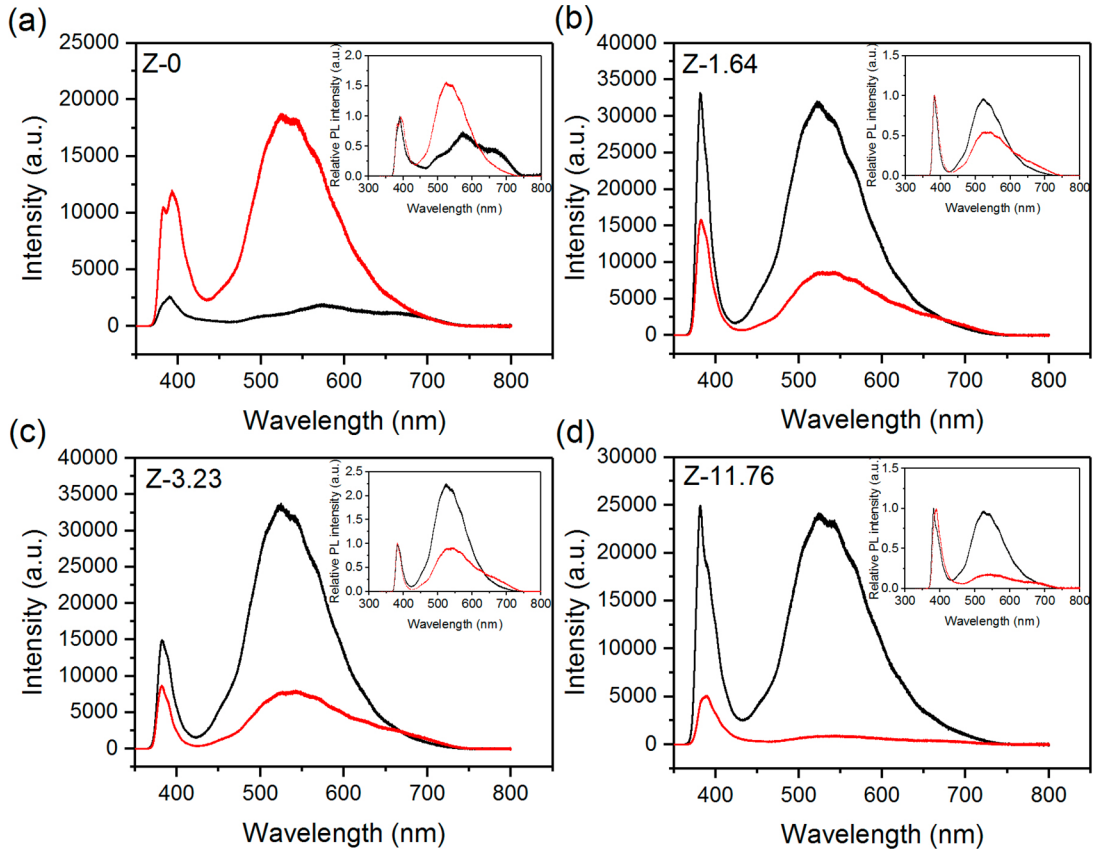

Figure 6. Photoluminescence spectra of as-prepared (black line) and annealed (red line) ZnO films at the additional volumes of acetic acid being (a) 0 mL (0 vol %), (b) 1 mL (1.64 vol %), (c) 2 mL (3.23 vol %), and (d) 8 mL (11.76 vol %) recorded under an excitation wavelength of 325 nm. Inset figures are normalized with respect to the maximum intensity of the NBE band at 380 nm.

due to exposed {001} facets. The absorption spectra of as-prepared thin films treated with acetic acid is similar. However, Z-3.23 provided the highest photocatalytic activity resulting from polar facets of the film.

It is worth noting that cycle experiments resulted in a significant drop of the initial ξ values of the as-deposited films. A consistent drop of activity during cycle experiments is typically attributed to surface poisoning due to carbon contamination during the photodegradation of organic pollutants. During our studies, however, the ZnO films remained active, showing constant ξ values, within error margins, after the first run (Figure 5b). This observation suggests that the initial enhanced values could be related to structural features or extrinsic properties, such as oxygen vacancies that may be depleted during reaction, although partial surface deactivation of the films cannot be ruled out. Further unusual behavior was observed upon annealing of the as-deposited films to 500 °C for 6 h in air. This annealing treatment is often performed to either enhance crystallinity or clean surfaces of potential carbon contamination, and it is usually reflected in a slight improvement in photocatalytic efficiency. Surprisingly, only the untreated sample showed an improved activity after annealing (Figure 5c) while the ξ values of the acid-treated samples dropped significantly. It is important to note that the physical properties of the samples did not change noticeably after annealing, as evidenced by XRD and SEM analysis (Figures S2 and S3).

Insight into the photocatalytic behavior of the ZnO films was sought upon exploration of structural defects using photoluminescence (PL) spectroscopy. The PL spectra of ZnO films commonly exhibit two main features: a near-band-edge (NBE) emission band around 375 nm and a deep-level emission (DLE) broad band in the visible range (Figure 6).[40,57]

The UV emission band is due to the recombination of photogenerated electrons from the conduction band to the valence band.[58] In general, strong PL indicates a high degree of recombination of photogenerated carriers and therefore suggesting low photoactivity. The position of free recombination of excitons at 375 nm (3.31 eV) was in good agreement with the E_{bg} values estimated for our films (Table 1). The deep-level emission (DLE) broad band centered at 550 nm (2.3 eV) is thought to be due to defects such as single ionized oxygen vacancies, oxygen antisites, zinc vacancies, and oxygen deficiency.[4,59−63] The concentration of oxygen vacancies can be estimated by taking the ratio between visible and UV emission intensity (I_{vis}/I_{UV}).[4,5,64]

Oxygen vacancies can bind photoinduced electrons enhancing the separation of photogenerated excitons, thus promoting photocatalytic efficiency.[65,66] Therefore, as a general rule, a higher I_{vis}/I_{UV} ratio (i.e., high concentration of defects) may be indicative of enhanced photocatalytic efficiency. Figure 6 shows PL spectra (excitation wavelength of 325 nm) before and after the annealing of ZnO films at 500 °C in air. Close inspection of the figure revealed a relative drop in intensity of the DLE band (I_{vis}) relative to the NBE band (I_{UV}) after annealing of the acid-treated samples, with the untreated sample (Z-0) showing the opposite trend. This is highlighted

DOI: 10.1021/acsanm.9b00326
ACS Appl. Nano Mater. 2019, 2, 2881−2889

in the inset plots in Figure 6, which show the normalized PL spectra with reference to the maximum intensity of the corresponding NBE bands.

The change in the normalized I_{vis}, i.e., $\Delta I_{vis} = I_{vis}$(annealed) − I_{vis}(as-deposited), is plotted in Figure 7 against the corresponding change in ξ values as estimated before and after annealing of the samples.

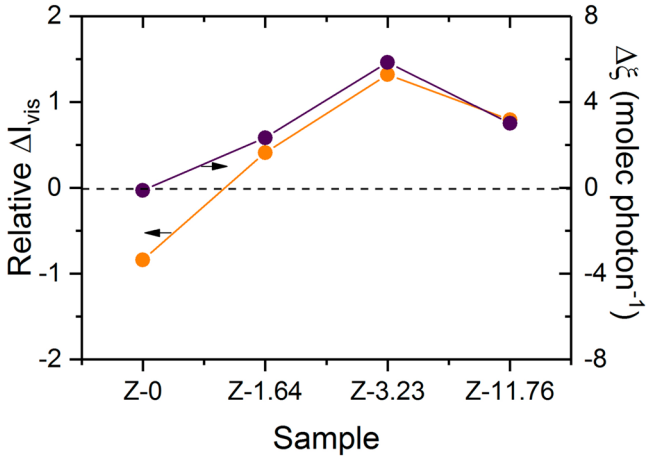

Figure 7. Trends of relative band intensity change, i.e., $\Delta I_{vis} = I_{vis}$(annealed) − I_{vis}(as-deposited), with respect to their corresponding NBE band maxima (I_{UV}) and change in ξ before and after annealing.

The close correlation between these trends, particularly in the case of the acid-treated samples (Z-1.64, Z-3.23, and Z-11.76), suggests that the initial enhanced photocatalytic efficiency of these ZnO films is indeed related to oxygen vacancies that are either depleted during the photocatalytic process or can heal upon exposure to air at high temperature.

4. CONCLUSION

Highly textured, defected ZnO thin films were grown via AACVD on SiO_2 barrier coated float glass. The addition of small volumes of acetic acid in the precursor solution had a huge impact on particle growth and film morphology, promoting lateral grain growth and exposing polar facets for an optimum photocatalytic performance. The initial formal efficiencies of the as-deposited films were found to decrease suddenly, either upon photodegradation of the organic pollutant or under annealing in air. This drop in activity was consistent with changes in photoluminescence spectroscopy and correlated to the depletion or healing of defects, likely oxygen vacancies. This encouraging result is a step forward toward the fabrication of optimized photocatalytic materials, and it calls for the implementation of synthesis strategies of high-surface-area photocatalysts with stable defects.

■ ASSOCIATED CONTENT

Supporting Information

The Supporting Information is available free of charge on the ACS Publications website at DOI: 10.1021/acsanm.9b00326.

Figures S1−S3 (PDF)

■ AUTHOR INFORMATION

Corresponding Author

*Fax (+44) 20-7679-7463; e-mail i.p.parkin@ucl.ac.uk.

ORCID

Premrudee Promdet: 0000-0002-4509-523X
Sanjayan Sathasivam: 0000-0002-5206-9558
Arreerat Jiamprasertboon: 0000-0002-8397-1149
Jian Guo: 0000-0001-8049-2567
Alaric Taylor: 0000-0001-6494-8309
Claire J. Carmalt: 0000-0003-1788-6971

Notes

The authors declare no competing financial interest.

■ ACKNOWLEDGMENTS

This work is supported by The Development and Promotion of Science and Technology Talents Project for a fellowship of P. Promdet. I.P.P. and C.J.C. thank EPSRC for grant EP/L0177709/1.

■ REFERENCES

(1) Hoffmann, M. R.; Martin, S. T.; Choi, W.; Bahnemann, D. W. Environmental Applications of Semiconductor Photocatalysis. *Chem. Rev.* **1995**, *95* (1), 69−96.
(2) Yassitepe, E.; Yatmaz, H. C.; Öztürk, C.; Öztürk, K.; Duran, C. Photocatalytic Efficiency of ZnO Plates in Degradation of Azo Dye Solutions. *J. Photochem. Photobiol., A* **2008**, *198* (1), 1−6.
(3) Xie, W.; Li, Y.; Sun, W.; Huang, J.; Xie, H.; Zhao, X. Surface Modification of ZnO with Ag Improves Its Photocatalytic Efficiency and Photostability. *J. Photochem. Photobiol., A* **2010**, *216* (2−3), 149−155.
(4) Wang, J.; Yang, J.; Li, X.; Feng, B.; Wei, B.; Wang, D.; Zhai, H.; Song, H. Effect of Surfactant on the Morphology of ZnO Nanopowders and Their Application for Photodegradation of Rhodamine B. *Powder Technol.* **2015**, *286* (3), 269−275.
(5) Zhang, X.; Qin, J.; Xue, Y.; Yu, P.; Zhang, B.; Wang, L.; Liu, R. Effect of Aspect Ratio and Surface Defects on the Photocatalytic Activity of ZnO Nanorods. *Sci. Rep.* **2015**, *4*, 4−11.
(6) Wang, Z.; Liu, S.; Zhang, J.; Yan, J.; Zhao, Y.; Mahoney, C.; et al. Photocatalytic Active Mesoporous Carbon/ZnO Hybrid Materials from Block Copolymer Tethered ZnO Nanocrystals. *Langmuir* **2017**, *33*, 12276−12284.
(7) Venkatesha, T. G.; Arthoba Nayaka, Y.; Viswanatha, R.; Vidyasagar, C. C.; Chethana, B. K. Electrochemical Synthesis and Photocatalytic Behavior of Flower Shaped ZnO Microstructures. *Powder Technol.* **2012**, *225*, 232−238.
(8) Hong, R. Y.; Li, J. H.; Chen, L. L.; Liu, D. Q.; Li, H. Z.; Zheng, Y.; Ding, J. Synthesis, Surface Modification and Photocatalytic Property of ZnO Nanoparticles. *Powder Technol.* **2009**, *189* (3), 426−432.
(9) Xie, J.; Li, Y.; Zhao, W.; Bian, L.; Wei, Y. Simple Fabrication and Photocatalytic Activity of ZnO Particles with Different Morphologies. *Powder Technol.* **2011**, *207* (1−3), 140−144.
(10) Maeda, K.; Takata, T.; Hara, M.; Saito, N.; Inoue, Y.; Kobayashi, H.; Domen, K. *J. Am. Chem. Soc.* **2005**, *127*, 8286−8287.
(11) Yang, X.; Wolcott, A.; Wang, G.; Sobo, A.; Fitzmorris, R. C.; Qian, F.; Zhang, J. Z.; Li, Y. Nitrogen-Doped ZnO Nanowire Arrays for Photoelectrochemical Water Splitting. *Nano Lett.* **2009**, *9*, 2331−2336.
(12) Wang, M.; Ren, F.; Zhou, J.; Cai, G.; Cai, L.; Hu, Y. N Doping to ZnO Nanorods for Photoelectrochemical Water Splitting under Visible Light: Engineered Impurity Distribution and Terraced Band Structure. *Sci. Rep.* **2015**, *5*, 1−13.
(13) Huang, L.; Lau, S. P.; Yang, H. Y.; Leong, E. S. P.; Yu, S. F.; Prawer, S. Stable Superhydrophobic Surface via Carbon Nanotubes Coated with a ZnO Thin Film. *J. Phys. Chem. B* **2005**, *109* (16), 7746−7748.
(14) Sun, R.-D.; Nakajima, A.; Fujishima, A.; Watanabe, T.; Hashimoto, K. Photoinduced Surface Wettability Conversion of

ZnO and TiO $_2$ Thin Films. *J. Phys. Chem. B* **2001**, *105* (10), 1984−1990.
(15) Shoaee, S.; Briscoe, J.; Durrant, J. R.; Dunn, S. Acoustic Enhancement of Polymer/ZnO Nanorod Photovoltaic Device Performance. *Adv. Mater.* **2014**, *26* (2), 263−268.
(16) Leung, Y. H.; He, Z. B.; Luo, L. B.; Tsang, C. H. A.; Wong, N. B.; Zhang, W. J.; Lee, S. T. ZnO Nanowires Array P-n Homojunction and Its Application as a Visible-Blind Ultraviolet Photodetector. *Appl. Phys. Lett.* **2010**, *96*, 053102.
(17) Han, J.; Fan, F.; Xu, C.; Lin, S.; Wei, M.; Duan, X.; Wang, Z. L. ZnO Nanotube-Based Dye-Sensitized Solar Cell and Its Application in Self-Powered Devices. *Nanotechnology* **2010**, *21* (40), 405203.
(18) Liu, J.; Chen, X.; Wang, W.; Liu, Y.; Huang, Q.; Guo, Z. Self-Assembly of [1010] Grown ZnO Nanowhiskers with Exposed Reactive (0001) Facets on Hollow Spheres and Their Enhanced Gas Sensitivity. *CrystEngComm* **2011**, *13* (10), 3425.
(19) Mclaren, A.; Valdes-Solis, T.; Li, G.; Tsang, S. C. Shape and Size Effects of ZnO Nanocrystals on Photocatalytic Activity. *J. Am. Chem. Soc.* **2009**, *131* (35), 12540−12541.
(20) Jang, E. S.; Won, J. H.; Hwang, S. J.; Choy, J. H. Fine Tuning of the Face Orientation of ZnO Crystals to Optimize Their Photocatalytic Activity. *Adv. Mater.* **2006**, *18* (24), 3309−3312.
(21) Ali, T. T.; Narasimharao, K.; Parkin, I. P.; Carmalt, C. J.; Sathasivam, S.; Basahel, S. N.; Bawaked, S. M.; Al-Thabaiti, S. A. Effect of Pretreatment Temperature on the Photocatalytic Activity of Microwave Irradiated Porous Nanocrystalline ZnO. *New J. Chem.* **2015**, *39* (1), 321−332.
(22) Ikizler, B.; Peker, S. M. Effect of the Seed Layer Thickness on the Stability of ZnO Nanorod Arrays. *Thin Solid Films* **2014**, *558*, 149−159.
(23) Ikizler, B.; Peker, S. M. Synthesis of TiO_2coated ZnO Nanorod Arrays and Their Stability in Photocatalytic Flow Reactors. *Thin Solid Films* **2016**, *605*, 232−242.
(24) Feng, W.; Chen, J.; Hou, C. Growth and Characterization of ZnO Needles. *Appl. Nanosci.* **2014**, *4* (1), 15−18.
(25) Yang, J. L.; An, S. J.; Park, W. I.; Yi, G.-C.; Choi, W. Photocatalysis Using ZnO Thin Films and Nanoneedles Grown by Metal-Organic Chemical Vapor Deposition. *Adv. Mater.* **2004**, *16* (18), 1661−1664.
(26) Mihailova, I.; Gerbreders, V.; Tamanis, E.; Sledevskis, E.; Viter, R.; Sarajevs, P. Synthesis of ZnO Nanoneedles by Thermal Oxidation of Zn Thin Films. *J. Non-Cryst. Solids* **2013**, *377*, 212−216.
(27) Tak, Y.; Yong, K.; Park, C. Selective Growth of ZnO Nanoneedles on Si Substrates by Metalorganic Chemical Vapor Deposition. *J. Cryst. Growth* **2005**, *285* (4), 549−554.
(28) Liu, Y.; Xu, W.; Shan, Y.; Xu, H. High Reactivity of the ZnO(0001) Polar Surface: The Role of Oxygen Adatoms. *J. Phys. Chem. C* **2017**, *121* (29), 15711−15718.
(29) Chen, C.; Yu, B.; Liu, J.; Dai, Q.; Zhu, Y. Investigation of ZnO Films on Si < 111> Substrate Grown by Low Energy O+ Assisted Pulse Laser Deposited Technology. *Mater. Lett.* **2007**, *61* (14−15), 2961−2964.
(30) Ko, H. J.; Hong, S. K.; Chen, Y.; Yao, T. A Challenge in Molecular Beam Epitaxy of ZnO: Control of Material Properties by Interface Engineering. *Thin Solid Films* **2002**, *409* (1), 153−160.
(31) Feng, L.; Liu, A.; Liu, M.; Ma, Y.; Wei, J.; Man, B. Fabrication and Characterization of Tetrapod-like ZnO Nanostructures Prepared by Catalyst-Free Thermal Evaporation. *Mater. Charact.* **2010**, *61* (1), 128−133.
(32) Chien, F. S. S.; Wang, C. R.; Chan, Y. L.; Lin, H. L.; Chen, M. H.; Wu, R. J. Fast-Response Ozone Sensor with ZnO Nanorods Grown by Chemical Vapor Deposition. *Sens. Actuators, B* **2010**, *144* (1), 120−125.
(33) Joshi, S.; Parmar, M.; Rajanna, K. A Novel Gas Flow Sensing Application Using Piezoelectric ZnO Thin Films Deposited on Phynox Alloy. *Sens. Actuators, A* **2012**, *187*, 194−200.
(34) Sathasivam, S.; Arnepalli, R. R.; Kumar, B.; Singh, K. K.; Visser, R. J.; Blackman, C. S.; Carmalt, C. J. Solution Processing of GaAs Thin Films for Photovoltaic Applications. *Chem. Mater.* **2014**, *26* (15), 4419−4424.
(35) Powell, M. J.; Carmalt, C. J. Aerosols: A Sustainable Route to Functional Materials. *Chem. - Eur. J.* **2017**, DOI: 10.1002/chem.201786261.
(36) Marchand, P.; Hassan, I. A.; Parkin, I. P.; Carmalt, C. J. Aerosol-Assisted Delivery of Precursors for Chemical Vapour Deposition: Expanding the Scope of CVD for Materials Fabrication. *Dalton Trans.* **2013**, *42* (26), 9406−9422.
(37) Chadwick, N.; Sathasivam, S.; Kafizas, A.; Bawaked, S. M.; Obaid, A. Y.; Al-Thabaiti, S.; Basahel, S. N.; Parkin, I. P.; Carmalt, C. J. Combinatorial Aerosol Assisted Chemical Vapour Deposition of a Photocatalytic Mixed SnO 2/TiO 2 Thin Film. *J. Mater. Chem. A* **2014**, *2* (14), 5108−5116.
(38) Alotaibi, A. M.; Sathasivam, S.; Williamson, B. A. D.; Kafizas, A.; Sotelo-Vazquez, C.; Taylor, A.; Scanlon, D. O.; Parkin, I. P. Chemical Vapor Deposition of Photocatalytically Active Pure Brookite TiO_2 Thin Films. *Chem. Mater.* **2018**, *30* (4), 1353−1361.
(39) Hassan, I. A.; Ratnasothy, A.; Bhachu, D. S.; Sathasivam, S.; Carmalt, C. J. The Effect of Solvent on the Morphology of Indium Oxide Deposited by Aerosol-Assisted Chemical Vapour Deposition. *Aust. J. Chem.* **2013**, *66* (10), 1274−1280.
(40) Liqiang, J.; Yichun, Q.; Baiqi, W.; Shudan, L. Review of photoluminescence performance of nano-sized semiconductor materials and its relationships with photocatalytic activity. *Sol. Energy Mater. Sol. Cells* **2006**, *90*, 1773−1787.
(41) Zheng, Y.; Chen, C.; Zhan, Y.; Lin, X.; Zheng, Q.; Wei, K.; Zhu, J.; Zhu, Y. Luminescence and Photocatalytic Activity of ZnO Nanocrystals: Correlation between Structure and Property. *Inorg. Chem.* **2007**, *46* (16), 6675−6682.
(42) Guo, M. Y.; Ng, A. M. C.; Liu, F.; Djurišić, A. B.; Chan, W. K.; Su, H.; Wong, K. S. Effect of Native Defects on Photocatalytic Properties of ZnO. *J. Phys. Chem. C* **2011**, *115* (22), 11095−11101.
(43) Mittal, K. L. Adhesion Measurement of Thin Films. *Electrocomponent Sci. Technol.* **1976**, *3* (1), 21−42.
(44) Powell, M. J.; Quesada-Cabrera, R.; Travis, W. L.; Parkin, I. P. High-Throughput Synthesis of Core-Shell and Multi-Shelled Materials by Fluidised Bed Chemical Vapour Deposition. Case Study: Double-Shell Rutile-Anatase Particles. *J. Mater. Chem. A* **2015**, *3* (33), 17241−17247.
(45) Quesada-Cabrera, R.; Sotelo-Vazquez, C.; Bear, J. C.; Darr, J. A.; Parkin, I. P. Photocatalytic Evidence of the Rutile-to-Anatase Electron Transfer in Titania. *Adv. Mater. Interfaces* **2014**, *1* (6), 1400069.
(46) Chen, S.; Wilson, R. M.; Binions, R. Synthesis of Highly Surface-Textured ZnO Thin Films by Aerosol Assisted Chemical Vapour Deposition. *J. Mater. Chem. A* **2015**, *3* (11), 5794−5797.
(47) Tian, Z. R.; Voigt, J. A.; Liu, J.; Mckenzie, B.; Mcdermott, M. J.; Rodriguez, M. A.; Konishi, H.; Xu, H. Complex and Oriented ZnO Nanostructures. *Nat. Mater.* **2003**, *2* (12), 821−826.
(48) Zhou, X.; Xie, Z.-X.; Jiang, Z.-Y.; Kuang, Q.; Zhang, S.-H.; Xu, T.; Huang, R.-B.; Zheng, L.-S. Formation of ZnO Hexagonal Micro-Pyramids: A Successful Control of the Exposed Polar Surfaces with the Assistance of an Ionic Liquid. *Chem. Commun.* **2005**, *1* (44), 5572.
(49) Herring, N. P.; Abouzeid, K.; Mohamed, M. B.; Pinsk, J.; El-Shall, M. S. Formation Mechanisms of Gold-Zinc Oxide Hexagonal Nanopyramids by Heterogeneous Nucleation Using Microwave Synthesis. *Langmuir* **2011**, *27* (24), 15146−15154.
(50) Nicholas, N. J.; Franks, G. V.; Ducker, W. A. Selective Adsorption to Particular Crystal Faces of ZnO. *Langmuir* **2012**, *28* (18), 7189−7196.
(51) Peng, Y.; Ji, J.; Zhao, X.; Wan, H.; Chen, D. Preparation of ZnO Nanopowder by a Novel Ultrasound Assisted Non-Hydrolytic Sol-Gel Process and Its Application in Photocatalytic Degradation of C.I. Acid Red 249. *Powder Technol.* **2013**, *233*, 325−330.
(52) Vallejos, S.; Pizúrová, N.; Gràcia, I.; Sotelo-Vazquez, C.; Čechal, J.; Blackman, C.; Parkin, I.; Cané, C. ZnO Rods with Exposed {100} Facets Grown via a Self-Catalyzed Vapor-Solid Mechanism and

DOI: 10.1021/acsanm.9b00326
ACS Appl. Nano Mater. 2019, 2, 2881−2889

Their Photocatalytic and Gas Sensing Properties. *ACS Appl. Mater. Interfaces* **2016**, *8* (48), 33335−33342.
(53) Li, D.; Huang, J. F.; Cao, L. Y.; Li, J. Y.; Ouyang, H. B.; Yao, C. Y. Microwave Hydrothermal Synthesis of Sr2+doped ZnO Crystallites with Enhanced Photocatalytic Properties. *Ceram. Int.* **2014**, *40* (2), 2647−2653.
(54) Shaban, M.; El Sayed, A. M. Effects of Lanthanum and Sodium on the Structural, Optical and Hydrophilic Properties of Sol-Gel Derived ZnO Films: A Comparative Study. *Mater. Sci. Semicond. Process.* **2016**, *41*, 323−334.
(55) Muchuweni, E.; Sathiaraj, T. S.; Nyakotyo, H. Synthesis and Characterization of Zinc Oxide Thin Films for Optoelectronic Applications. *Heliyon.* **2017**, *3* (4), No. e00285.
(56) Mills, A.; Wang, J. Simultaneous Monitoring of the Destruction of Stearic Acid and Generation of Carbon Dioxide by Self-Cleaning Semiconductor Photocatalytic Films. *J. Photochem. Photobiol., A* **2006**, *182* (2), 181−186.
(57) Djurišić, A. B.; Choy, W. C. H.; Roy, V. A. L.; Leung, Y. H.; Kwong, C. Y.; Cheah, K. W.; Rao, T. K. G.; Chan, W. K.; Lui, H. F.; Surya, C. Photoluminescence and Electron Paramagnetic Resonance of ZnO Tetrapod Structures. *Adv. Funct. Mater.* **2004**, *14* (9), 856−864.
(58) Ren, L.; Tian, T.; Li, Y.; Huang, J.; Zhao, X. High-Performance UV Photodetection of Unique ZnO Nanowires from Zinc Carbonate Hydroxide Nanobelts. *ACS Appl. Mater. Interfaces* **2013**, *5* (12), 5861−5867.
(59) Chen, D.; Wang, Z.; Ren, T.; Ding, H.; Yao, W.; Zong, R.; Zhu, Y. Influence of Defects on the Photocatalytic Activity of ZnO, 2014.
(60) Kwok, W. M.; Djurišić, A. B.; Leung, Y. H.; Chan, W. K.; Phillips, D. L. Time-Resolved Photoluminescence from ZnO Nanostructures. *Appl. Phys. Lett.* **2005**, *87* (22), 223111.
(61) Studenikin, S. A.; Golego, N.; Cocivera, M. Fabrication of Green and Orange Photoluminescent, Undoped ZnO Films Using Spray Pyrolysis. *J. Appl. Phys.* **1998**, *84* (4), 2287−2294.
(62) Li, D.; Leung, Y. H.; Djurišić, A. B.; Liu, Z. T.; Xie, M. H.; Shi, S. L.; Xu, S. J.; Chan, W. K. Different Origins of Visible Luminescence in ZnO Nanostructures Fabricated by the Chemical and Evaporation Methods. *Appl. Phys. Lett.* **2004**, *85* (9), 1601−1603.
(63) Tam, K. H.; Cheung, C. K.; Leung, Y. H.; Djurišić, A. B.; Ling, C. C.; Beling, C. D.; Fung, S.; Kwok, W. M.; Chan, W. K.; Phillips, D. L.; Ding, L.; Ge, W. K. Defects in ZnO Nanorods Prepared by a Hydrothermal Method. *J. Phys. Chem. B* **2006**, *110* (42), 20865−20871.
(64) Drouilly, C.; Krafft, J. M.; Averseng, F.; Casale, S.; Bazer-Bachi, D.; Chizallet, C.; Lecocq, V.; Vezin, H.; Lauron-Pernot, H.; Costentin, G. ZnO Oxygen Vacancies Formation and Filling Followed by in Situ Photoluminescence and in Situ EPR. *J. Phys. Chem. C* **2012**, *116* (40), 21297−21307.
(65) Yun, H. J.; Lee, H.; Joo, J. B.; Kim, W.; Yi, J. Influence of Aspect Ratio of TiO 2 Nanorods on the Photocatalytic Decomposition of Formic Acid. *J. Phys. Chem. C* **2009**, *113* (8), 3050−3055.
(66) Kong, M.; Li, Y.; Chen, X.; Tian, T.; Fang, P.; Zheng, F.; Zhao, X. Tuning the Relative Concentration Ratio of Bulk Defects to Surface Defects in TiO_2nanocrystals Leads to High Photocatalytic Efficiency. *J. Am. Chem. Soc.* **2011**, *133* (41), 16414−16417.

DOI: 10.1021/acsanm.9b00326
ACS Appl. Nano Mater. 2019, 2, 2881−2889